MISR instrument development and test status

Carol Bruegge, Valerie Duval, Nadine Chrien, Robert Korechoff
Jet Propulsion Laboratory, California Institute of Technology
4800 Oak Grove Dr., Pasadena, Ca. 91109

ABSTRACT

MISR will provide global data sets from Earth orbit using nine discrete cameras, each viewing at unique view directions. The design of this instrument is complete and has been refined following assembly and testing of an engineering model. The engineering model has been invaluable in identifying erectable design flaws, in resolving subsystem interface issues early in the program, and in providing the science team with as-built performance data to be used in the algorithm development. MISR will fly with an on-board calibrator consisting of Spectralon diffuse panels and photodiode detector standards. Both the use of SpectraIon and flight detector standards have been developed by the MISR team. Currently the engineering team is assembling and testing the flight cameras, and the data teams are preparing for the. post-launch geometric and radiometric calibration of the instrument, as well as developing algorithms to provide the science products. With a 3.3 Mb orbital average data rate, and global coverage each nine days, processing will be automated and standardize. Deliverables include. calibrated, registered data sets, as well as aerosol/ land surface, and cloud parameters.

1. INTRODUCTION

MISR will acquire systematic multi-angle imagery to monitor top-of-atmosphere and surface reflectances on a global basis, and to characterize the shortwave radiative properties of aerosols, clouds, and surface scenes. Data from the MISR experiment will enable advances in a number of areas concerning global change

- _ High resolution bidirectional reflectances will be used in cloud classification, and the spatial and temporal variability of cloud hemispheric reflectance will be determined. Stereoscopic measurements will be used to retrieve cloud-top elevations. These data will help discern the role of different clouds types in the Earth's energy balance.
- Aerosols. Multi-angle radiance data will be used to determine aerosol optical depth, and to identify particle composition and size distribution. These data will enable a global study of the role of aerosols on the energy budget, and wilt provide data used for atmospheric correction of surface imagery.
- Land surface. Atmospherical y-corrected surface bidirectional reflectances will be used to estimate surface hemispheric reflectance, an important climate variable, and to characterize vegetation canopy structures, These data will be important for investigating the effect of land surface processes on climate.
- Oceans. MISR will provide data to support ocean biological productivity studies in regions of low phytoplankton pigment concentrations, such as much of the tropical oceans.

2. Instrument

The MISR instrument has been designed at built by the Jet Propulsion Laboratory (JPL), to be launched in 1998 as one of five instruments on the first Earth Observing System platform (EOS-AM), will fly in a 705 km (440 mile) sun-synchronous descending polar orbit, with an equatorial crossing time of 10:30 a.m. The instrument wilt be used to produce registered global data sets from nine cameras (spanning a range of view angles from nadir to ±70.5°) and four spectral bands, The time separation from observation of a single ground target from the forward most camera to the aftmost view is 7 minutes. Within this time the spacecraft covers a ground track of 2800 km and the instrument images in a swath width of 378 km. Each of the nine cameras images in four spectral bands, nominally centered at 443,555,670, and 865 nm. Spectral bandwidths vary between 15 and 25 nm. A CCD *line array,* 1504 active elements per line, underlie each of the four interference filter strips. At the Earth's surface each detector element produces a data pixel with a cross-track spatial sampling interval of 275 m (250 m for the nadir camera). A schematic of the views to Earth is shown below. The camera which views a given direction is depicted. The naming convention includes the lens type (A-D) and (f)orward, (n)adir or (a)ft designators.

Satellite Remote Sensing 11, Proc. SPIE 2583, Paris, France. (August 25, 1995)

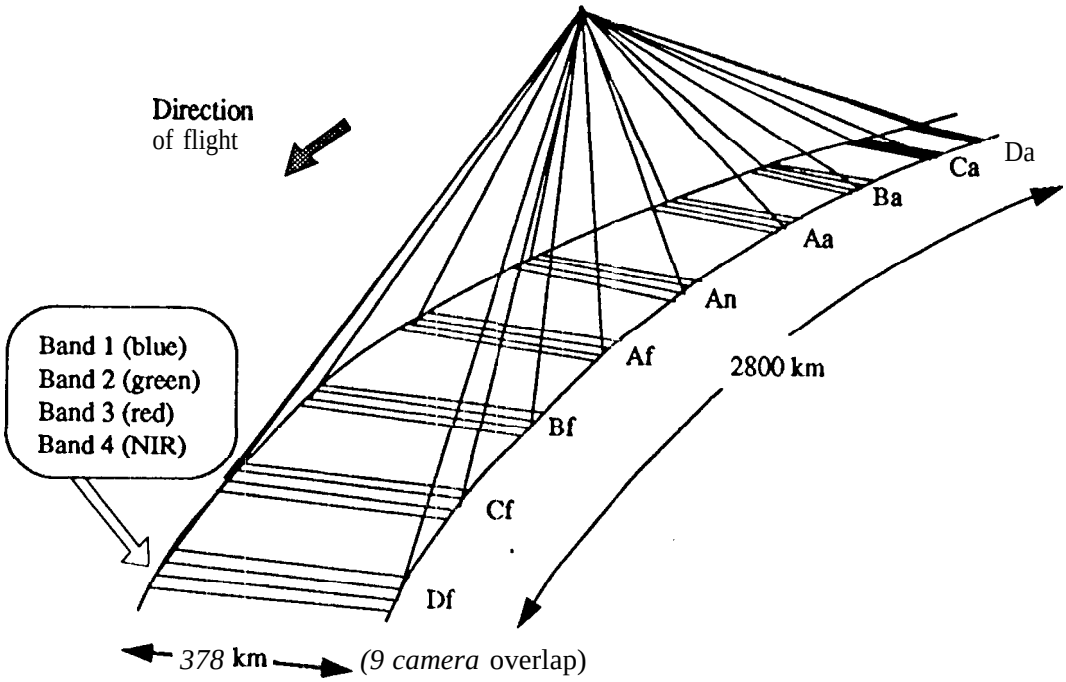

Figure 1. MISR camera projections to Earth.

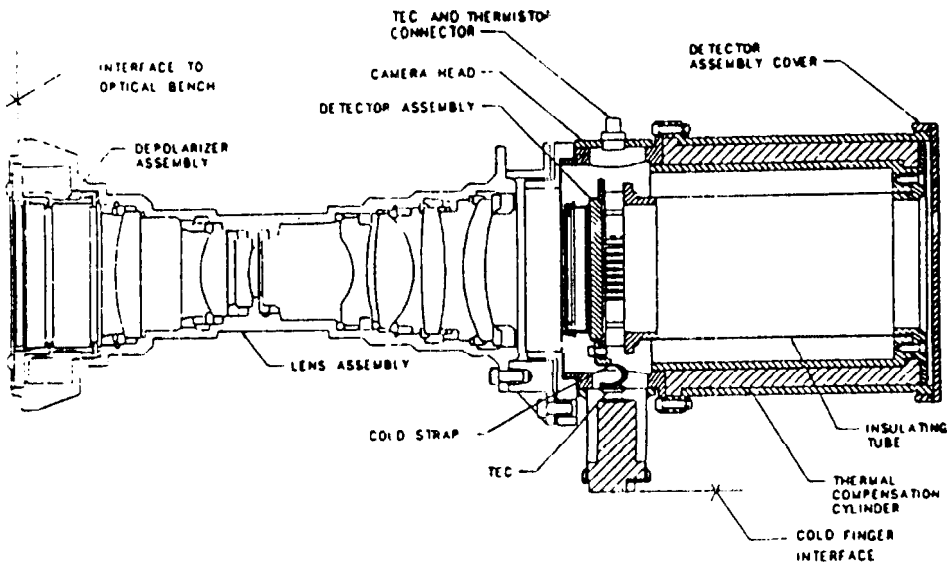

Figure 2. Camera layout.

high signal levels. This is an acceptable trade-off as photon noise is the dominant error source at the higher radiometric levels. During ground data processing the square-root encoding is reversed. This produces a DN data set which is linear related to incident radiance. (At this time the DN are also padded to 16-bit filling, simply to package into machine words). On-board data averaging of 4x4 (crosstrack x alongtrack), 1x4, and 2x2 pixels is part of the routine global observation plan, the specific camera configuration being camera and band dependent. A small number of specific sites (-100), defined by the science, calibration, and data validation teams, are targeted and viewed in an unaveraged mode on a routine or event-driven basis, depending on the scene. Thus the science investigator most typically works with 1.1 km pixels, but has routine observations at higher resolution.

2.3 On-Board Calibrator

For both the preflight and in-flight calibrations MISR output are radion Metrically calibrated using a spatially uniform source whose radiant output is determined using detector standards. Source standards rely on a series of radiometric comparisons, as provided by the National Institute of Standards and Technology (NIST) or other standards laboratory, through a lamp vendor, and to the instrument flat-field calibration source. Conversely, detector standards are based upon manufacturing knowledge of photon to electron conversion efficiency, filter transmittance, and acceptance cone of illumination. It is believed that the MISR detector standards provide greater radiometric accuracy than would be obtained using source standards. During preflight testing, an integrating sphere and laboratory photodiode standards are utilized to achieve the radiometric calibration of the camera.% In-flight, MISR is calibrated using an On-Board Calibrator (OBC) that consists of two Spectralon diffuse calibration panels, High Quantum Efficiency (HQE) diodes in a trapped configuration, and single (not trapped) radiation-resistant PIN diodes, including one mounted to a goniometer arm to provide angular characterization of the diffuse panels. Figure 3 shows the location of these elements with respect to the optical bench structure.

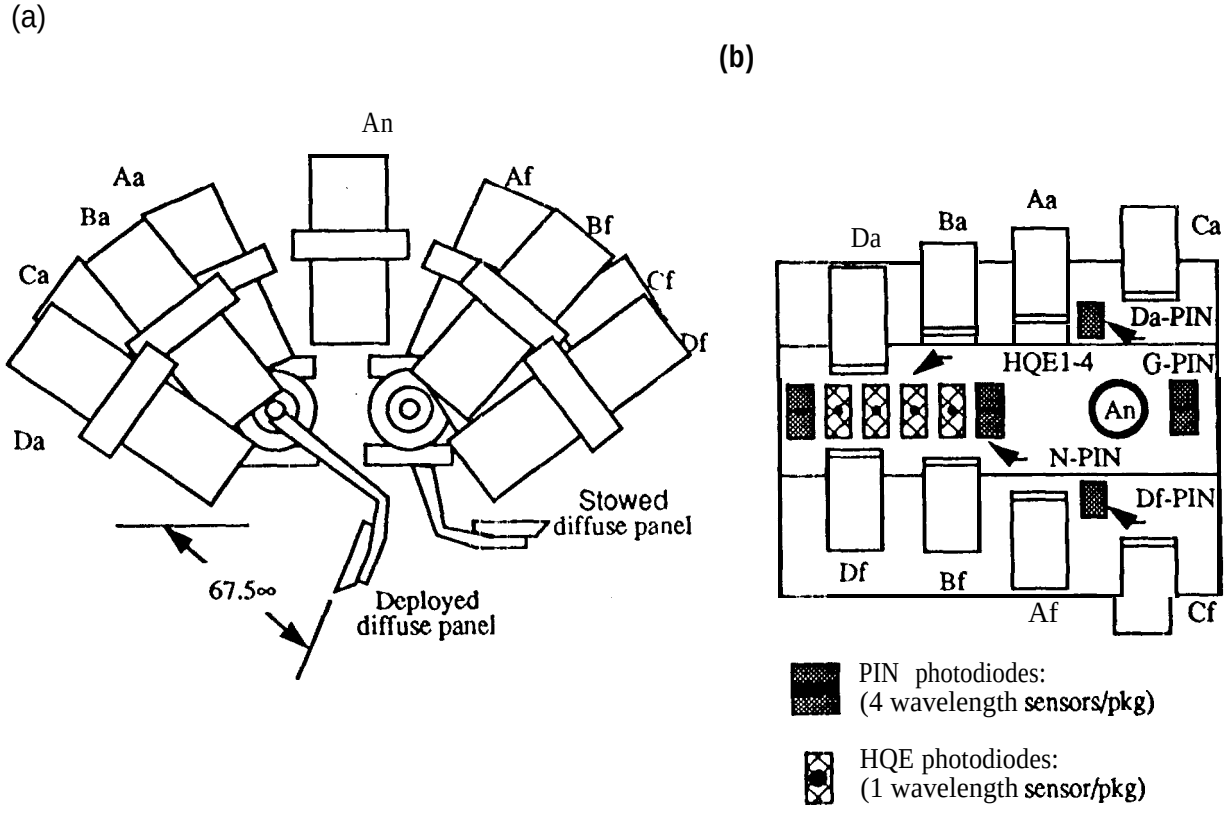

Figure 3. Location of a) the calibration panels and b) photodiodes on the optical bench.

2.1 Camera Design

Each MISR camera consists of a lens barrel and a camera head which houses the focal plane structure and to which is attached the CCD driver electronics. A camera layout is shown in Figure 2. The design is superachromatic (having a common focus at three MISR wavelengths) and thermally compensate for focus. It is a seven-element telecentric Biotar form. (In the telecentric design, the chief rays exit the cameras nearly parallel to the optical axis, independent of location in the field of view, with the benefit that the bandpass of the focal plane interference filters is nearly constant across the field). An additional benefit of the telecentric design is that optical transmittance is only a weak function ($\cos^{-1}\theta$) of field angle 8. In order to meet the system radiometric accuracy requirements, a double-plate Lyot depolarizer is incorporated into each of the cameras in order to scramble the polarization state. The effectiveness of Lyot depolarizers is dependent on the spectral bandwidth as well as the spectral band shape, They are most effective for Gaussian-like band shapes. Thus, the MISR filters are specified to have Gaussian band shape profiles in order to optimize the performance of the Lyot depolarizers. The mosaic filter consists of four separate filter sticks epoxied into a single structure. When installed into the CCD package each of the four CCD line arrays sees a different color. Ion assisted deposition (IAD) technology has been utilized to insure stable, durable coatings. Manufacturing the passband and blocking layers on separate substrates prevents cost from being prohibitive. After the coating runs the two substrates are bonded together, with the coatings to the interior. Optical masks are incorporated into the assembly to prevent white-light leakage through the inter-filter epoxy bonds. The filter layouts are given in the companion paper[2].

The MISR CCD architecture consists of four line arrays on a common piece of silicon with a spacing of 160 μm (6.3 roils) center-to-center. The filter defining the four optical bandpasses is aligned with the CCDs, but displaced above the focal plane by 38 μm (1.5 roil), The package has a laser welded window, is back filled with argon, and hermetically sealed. The hermetic package prevents contamination of the falter and CCD elements, eliminates humidity, and improves stability. Integration time for each line array can be controlled independently. This allows for different integration times in different bandpasses in order to equalize radiometric performance and maximize signal-to-noise ratio. The arrays are operated at 50 kilopixels per second with a 40.8 msec line repeat time to provide 275 m of along-track separation between successive lines. The MISR CCD'S have a "thin-poly" design, a new technology developed to increase the detectors' sensitivity to wavelengths shorter than 500 nm. The detector is cooled to -5° C with a single-stage Thermo-Electric Cooler (TEC). Temperature stability is within ±0.1° C, accomplished by computer cent.ml of a heater.

2.2 Instrument subsystems

The cameras are mounted to an optical bench at their front (light entrance) end with the detector end cantilevered into the instrument cavity. The Primary Support Structure enclosure walls are designed to maintain rigid support for the optical bench and provides kinematic attachment to the spacecraft. In addition, it provides a structural mount for the passive radiators located on the nadir-facing side of the instrument, houses the instrument system electronics and the flight computers, and incorporates optical baffles to keep specular glints from neighboring instruments from illuminating MISR's optical calibration surfaces.

The MISR electronics fall into three general areas: camera electronics, system electronics, and calibration electronics. Each camera is relatively autonomous with its own power supply and serial data interfaces. The camera electronics can stand alone through most testing and camera calibration. The design insures that if an in-flight failure occurs in a camera's electronics it is not allowed to propagate to another camera or to the system electronics. The camera digital electronics provide interfaces to the system electronics controlling the camera as well as all the drive and timing signals to the CCD focal plane. The signal chain amplifies and converts the CCD video into 14 bit digital numbers, The system digital electronics' main function is to interface the instrument to the platform. The system electronics also provide the high speed data interface, control inputs to the cameras, control power throughout the instrument, and control all of the mechanisms. A system circuit measures system-wide temperatures and voltages. All system electronics are redundant to avoid the possibility of a single point failure.

It has been demonstrated that a true 13-bit digital representation of the measured radiance is sufficient to meet the radiometric needs identified by the science team (less would incur increased quantization noise). Square-root encoding, as well as data averaging, is provided by the system electronics. These are implemented as a means of data compression, needed in order to meet the data rate constraints. Square-root encoding reduces quantization error at low signal levels at the expense of increased quantization error at

panels. Instrument geometric stability is characterized at the system level with use of a calibrated nine-collimator fixture which rests on the instrument optical bench during test Greater details on these tests are given in Bruegge, et al.'.

The specific tests conducted in each of the two thermal vacuum chambers are summarized in Table 1. After assembly a camera first goes to the Optical Characterization Chamber (OCC). External to this chamber resides a xenon lamp source which feeds a chamber-internal target wheel. At the target wheel, pinholes 35,50, 100, and *200pm in* size are available and are selected, according to the focal length of the camera under test, such that subpixel illumination is provided. The pinhole target is at the focus of a 1 m (40") collimator, allowing the camera to image onto the pinhole. As the camera is attached to a two axes gimbal, this pinhole. image can be scanned across the focal plane in either the downtrack or crosstrack directions. Further, the pinhole can be made to pass a finite spectral bandpass of light by prefiltering the source at the external lamp housing. During test the gimbal moves per a pre-programmed test plan to provide the data of interest. First data takes are conducted in ambient pressure and temperature conditions. All final OCC verifications and calibrations are done in vacuum, at multiple temperatures throughout the lens design range of 0° to 10° C. Testing is repeated pre and post dynamics and temperature survivability testing,

Table 1. Optical Characterization Chamber (OCC) tests. Here pinhole imaged onto camera via collimator and camera is mounted to two axis gimbal.

Test name.	Test description	Test deliverables
Boresight	Collimated beam illuminates camera at angle perpendicular to lens mounting flange (no gimbal skewing).	Provides verification that boresight is within ±8 pixels of CCD array center. Specific boresight location feeds into camera pointing model,
Point-source-function (PSF) response.	Scan accomplished by moving gimbal in 0.1 pixel steps at five field points. Repeated with white and filtered light.	Provides cross- and down-track line-spread function. Used to predict contrast target response, and available for at-launch contrast sharpening algorithm. Used to measure optical and electrical spectral crosstalk terms. Used to determine MTF and verify MTF specification (26% beginning of life at pixel sampling frequency).
Effective focal length	Same as above.	Best focus position determined at lens level of assembly. Camera assembled using appropriate shims to place detector at focus. Focus verified at camera through temperature range.
Distortion mapping	Same as above, but over entire CCD array. White light only.	Measures deviation of image point from h=EFL tan θ. Provides pixel IFOV knowledge to subpixel accuracy.
Stray light	Pinhole. illuminates various field points outside of the sensor field-of-view. Pinhole stationary to allow pixel summing.	Used to verify 10^{-5} out-of-field stray-light rejection.
Blooming, time response, and hysteresis studies	The pinhole source is shuttered to determine time response. Neutral density filters and camera integration time controlled saturated conditions (10 times full well).	Used to verify detector response specifications: time response for within dynamic range signals; saturation recovery in both the spatial and temporal dimensions.

The panels are deployed for calibration at monthly intervals, except at mission start when multiple observations are collected the first month, Over the North Pole, one panel will swing aftward to reflect diffuse sunlight into the fields-of-view of the aftward-looking and nadir cameras. Over the South Pole, the other panel will swing forward for calibration of the forward-looking and nadir cameras. Thus, the nadir camera will provide a link between the two sets of observations. By monitoring the panels with photodiode assemblies, and through consistency checks using overflight campaign data, slow changes in panel reflectance are allowable without compromising the calibration accuracy, since the photodiodes provide the primary standard. In addition to these panel views, the cameras will gather data over the dark Earth for three minutes each month. The dark-Earth data will establish the dark current spatial variability across the array. Dark current is expected to be slowly varying during the mission, gradually increasing due to particle radiation exposure.

The panels are required to have a high, near-Lambertian reflectance. These properties are needed to direct sufficient energy into the cameras to reach the upper end of the sensor dynamic range.. The Lam ıbertian property also facilitates knowledge of the radiance into the cameras, as the radiance is measured by photodiodes at a par titular panel view angle, and corrected for departure from Lambertian behavior. SpectraIon has been flight qualified by the MISR team (Bruegge, et. al, 1993; Stiegman, et al., 1993) for use as these in-orbit calibration targets. SpectraIon is a product of LabSphere (North Sutton, New Hampshire), and is composed of pure polytetrafluoroethylene (PTFE, or Teflon) polymer resin that is compressed into a hard porous white material using temperature and pressure sintering. No binders are used in the procedure.

The diffuse calibration targets will be monitored by three types of diodes: radiation-resistant PIN photodiodes and two types of High Quantum Efficiency (HQE) diodes. (Note: "PIN" is a description of the diode architecture where *p*, intrinsic, and *n* doped layers are stacked.) The radiation-resistant photodiodes will be fabricated four to a package, each diode filtered to a different MISR spectral band. Five such packages will be used. Two will view in the nadir direction, two in the Df and Da camera directions, and one package will be mechanized on a goniometric arm to monitor the angular reflectance properties of the panels.

The HQE's are in a "trap" configuration. Here three silicon photodiodes are arranged in a package so that light reflected from one diode is directed to *another* diode. The output of each diode is summed, resulting in near 100% quantum efficiency. A single spectral filter per package is used, and four such packages provide coverage at the four MISR wavelengths. One diode type will be used to obtain high quantum efficiency (QE) in the blue, and another type will be optimized for QE in the remaining three bands. The diodes have been specified to have an internal quantum efficiency exceeding 0.995, to have a front surface loss of less than 20%, to have a linearity of response better than 99.99% over an *equivalent reflectance* range of 5 to 100%, and to have SNR in excess of S00 at full scale. The equivalent reflectance parameter is used to specify instrument signal-to-noise requirements. This parameter is defined as: $\rho_{eq} = \pi L_\lambda / E_{0\lambda}$ where L_λ is the spectral radiance incident at the sensor while observing a given target, and $E_{0\lambda}$ is the spectral exo-atmospheric solar irradiance at wavelength λ. (Both L_λ and $E_{0\lambda}$ are band weighted over the passband response.) To convert an equivalent reflectance into radiance, therefore, $L_\lambda = E_{0\lambda} * \rho_{eq} / \pi$ where $E_{0\lambda}$ is the exo-atmospheric solar spectral irradiance, as given by the World Climate Research Programme[3].

The goniometer is a mechanized device which characterizes the relative diffuse panel radiance function with angle. It does so in a plane parallel to the spacecraft flight direction. A PIN package mounted to the goniometer arm swings through ±60° to allow panel characterization appropriate to the along-track camera angles.

2.4 Performance testing

Some degree of testing of MISR flight hardware is done at the component, camera, and system levels, as well as after shipment apd integration onto the spacecraft. The bulk of the performance data, however, are collected at the camera level of assembly. By characterizing each camera individually, testing can be spread sequentially over time and the test hardware is simplified. Camera testing is done using two MISR-dedicated thermal vacuum chambers. The camera-level approach to characterization also permits camera spares to be stored as calibrated, ready to fly hardware. The shorter system level tests are to be conducted in shared, more costfy facilities. Radiometric stability is verified at the system level of assembly by deploying and illuminating the flight diffuse

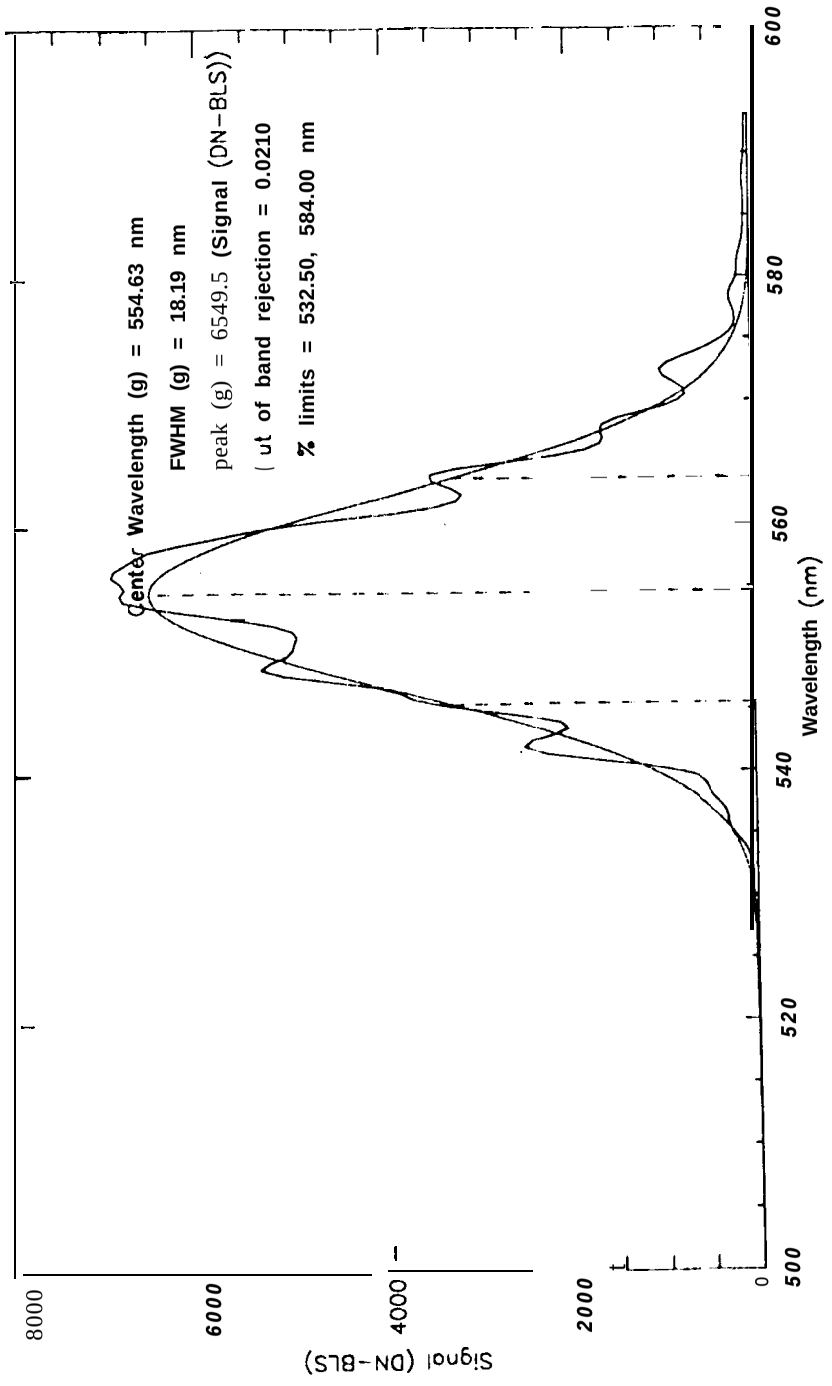

Figure 4. Gaussian fit to Band 4, center pixel of camera PFU312.

After testing in the OCC, a given camera is next moved to the Radiometric Characterization Chamber (RCC). This chamber has a 0.5 m (20") diameter window within it's door. Either a monochromator or integrating sphere are wheeled in front of the chamber, illuminating the camera through this window. Tables 2 and 3 describe tests conducted with these respective sources. For the spectral tests each pixel analyzed is parameterized in terms of a best-fit Gaussian to the in-band region, this being the 1 % points with respect to the peak. As the band profile was specified to be Gaussian, it is believed that this function best represents a simplified spectral response function, with pararneterization derived so as to preserve the integrated energy. As the MISR filters do have a finite out-of-band response, however, an equivalent parameterization is desired which accounts for the out-of-band energy. For this an equivalent square-band analysis is made. Out-of-band response beyond the limits of the monochromator (900 nm) is determined by use of a bandpass filter covering the 900 to 1100 nm region. This filter is used to prefilter the light while the camera views the integrating sphere. Figure depicts the Gaussian analysis for the center pixel of camera PFU3 12.

Table 2. Radiometric Characterization Chamber. Monochromator illuminates camera via window in chamber door.

Test name.	Test description	Test deliverables
SpectCal-In band	Scan monochromator from 400 to 900 nm in 0.5 nm steps, setting exit slit to 1 nm dispersion.	Gaussian in-band best-fit response parameters.
SpectCal-Out band	Scan monochromator from 400 to 900 nm in 10 nm steps, setting exit slit to 20 nm dispersion.	Equivalent square band response determined using moments analysis. Provides out-band rejection and response function for out-of-band correction to the flight data.

The integrating sphere used in these tests is 1.6 m (65") in diameter, has a 76x23 cm (30x9") exit port, and a 30 cm (12") external sphere with variable aperture. The main sphere is illuminated with use of eighteen *200* W bulbs and six 30 W bulbs; the satellite sphere has a single 200 W bulb. The sphere is sequenced through a number of lamp-on settings, allowing digital data to be collected at multiple radiometric levels. The coefficients in the. calibration equation are determined for each pixel using these data. A statistical approach called the Fidelity Analysis[1] is used LO fit a straight-line through the data, provide a measure of the uncertainty in this fit, and extrapolate the uncertainty to an arbitrary radiometric level. The gain and offset coefficients for cameraPFU312 are shown in Figures 4a and 4b, as well as the Fidelity interval uncertainty limits, Figure 4c. The gain and offset coefficients are a fit to the equation $L_\lambda = G(DN-DN_o)$, where L_λ [W $m^{-2} sr^{-1} \mu m^{-1}$] is the spectral output of the sphere, and DN_o [digital numbers (DN)] is output the extrapolated to a zero input radiance. Thus, with these pi xel coefficients the radiance of the scene cart be determined from the camera DN output. The uncertainty plot shows that there is about a 9% uncertainty in equivalent reflectance when the scene is low in reflectance (6%), and a 0.6% uncertainty at ρ_{eq}=100%. These give the uncertainty due to selected lamp levels, and camera dark current variations. In addition to this uncertainty, there is a systematic uncertainty of about 2% in the laboratory detector standards. Another contributor to radiometric error is the sphere drift between calibrations. By monitoring the sphere with an internal photodiode during testing, the total radiance and equivalent reflectance retrieval error cart be reduced such that we meet the 3% (1σ at ρ_{eq}=100%) uncertainty requirement.

Table 3. **Radiometric** Characterization Chamber. Integrating sphere **illuminates** camera via window in chamber door.

Test name.	Test description	Test deliverables
Light **transfer**	At fixed integrating sphere output level, ramp camera from 0.32 to 40.8 ms integration **times** (full **available** range).	**Determines** ADC gain, electronics linearity and linearity range, and desired camera integration time.
RadCal	Set the integrating sphere to one of 12 **precalibrated** output levels per band, Turn off bulbs and adjust external sphere aperture to sequence through all **preprogrammed** levels. Repeat for **all** 4 MISR spectral bands.	Provides the sensor absolute and relative **radiometric** calibration, radiance uncertainty, and signal-to-noise performance.
Doubling	At 9 **radiometric** levels, each achieved by two **identical** bulb groupings, acquire data with first, second, then and both bulb **sets** in turn.	Verifies linearity over sensor dynamic range where **radiometric** accuracy requirements are defined (ρ_{eq}=100%. to 5%).
Polarization	Rotate polarizing sheet (ambient trot).	Verifies camera ±1% polarization insensitivity **specification.**

3. Round robin **cross** comparison

Although the MISR integrating sphere is calibrated with use of detector standards the team has an interest in verifying the sphere output using independent techniques. The round-robin **cross-compar** ison experiment provided one such opportunity to do so. In August of 1994 severat members of the EOS calibration panel brought their **detector** standards to JPL. These were used to sequential y view the JPL integrating sphere. **Participating** were calibration scientists from the Optical **Sciences** Center, **Universit** y of **Arizona;** National Research Laboratory of Metrology **(NRLM),** the Japanese standards laboratory; and Goddard Space **Flight** Center **(GSFC).**

To calibrate the sphere, a UDT model **QED-200** is used **For** MISR **Bands 1** and 2. This detector **consists** of three inversion layer photodiodes arranged in a trapped configuration. For MISR Bands 3 and 4, a **Graesby** Electronics QED-150 is used. The latter standard is manufactured from **Hamamatsu** pen-n photodiodes, **also** positioned in a trapped configuration. During the round-robin experiment the standards were faltered with an **Optronics** catalog fitter. (Prior to the calibration of MISR flight **cameras** the standards are filtered using MISR laboratory filters, having **the** same band **profile** as the flight cameras). Next, the sphere was viewed by the University of Arizona portable **radiometer**[6]. As the sphere is **located** inside a dark **tent,** temperatures rose above the portable radiometers set point of **30°** C, by 1,8° C above the set point. Further uncertainties in the data reduction arose due to uncertainty in this instruments filter **transmittance.** For this reason the radiometer was calibrated during the Sep94 **SeaWiFs** SIRREX-3 experiment. **Finally,** the sphere was viewed by the **NRLM** radiometer[7]. This has a field-of-view of 0.387°, and is filtered at 650 nm, 50 nm width. Repeatability between the **08Aug95** and **09Aug95** observations of the sphere was better than 0.03% at all four **radiometric levels,** as measured by this latter instrument.

In order to **intercompare** observations from these **three** detectors, a means of extrapolating measurements at one particular instruments **bandpass,** to that observed by another instrument with **a** different band profile was needed. It was decided to use the JPL observations to calibrate a sphere output model, and in turn **compare** the visitor observations to this model. The utility of the" model was simply to provide the wavelength interpolator **needed** to **intercompare** the various spectral observations, **The** model used was: $L_\lambda \cdot \frac{\pi \vartheta_{bulb}}{\sigma T^4} \frac{\rho}{1-\rho(1-f)} \frac{L_{BB\lambda}}{\pi A_s}$, where

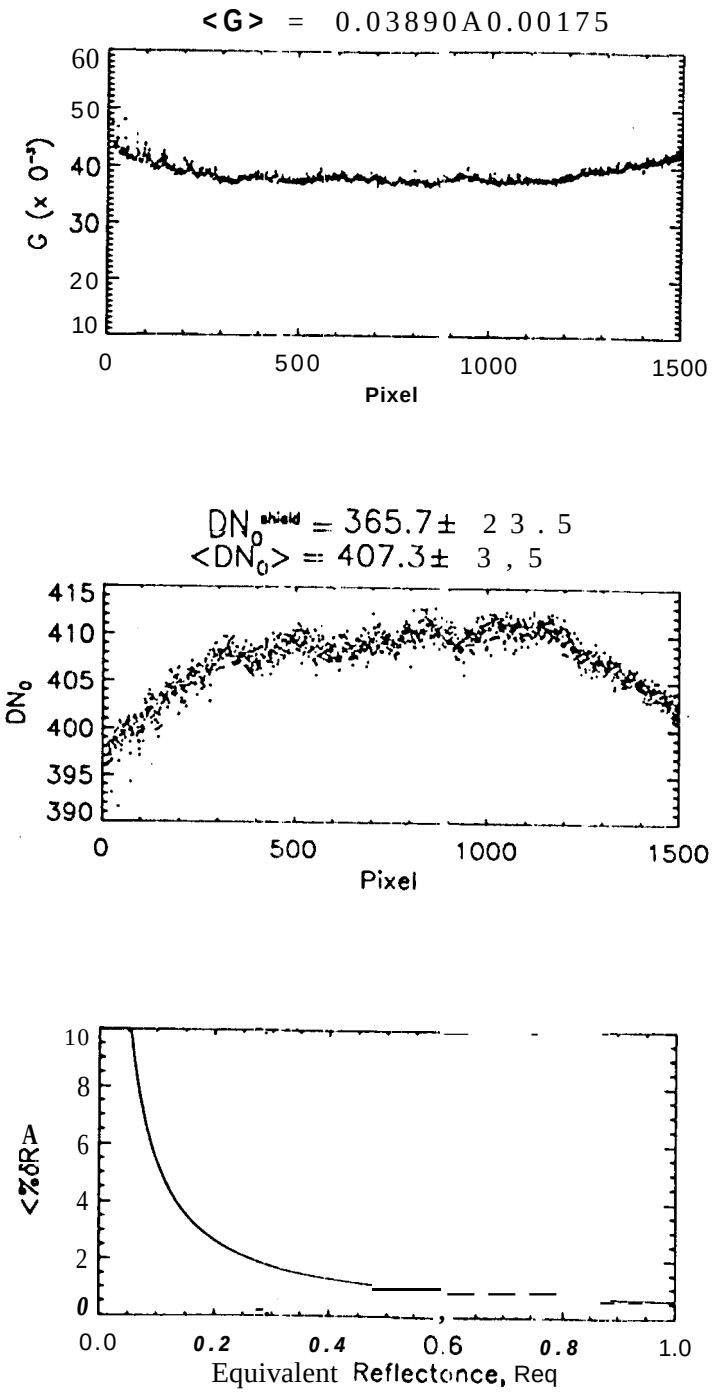

Figure 5. Gain and offset coefficients for Band 2, camera PFU312, with Fidelity Interval computed uncertainty.

3. Wehrli, C. (1985). Extraterrestrial Solar Spectrum. World Radiation Center (WRC). Davos-Dorf, Switzerland, WRC Publication No. 615, July.

4. Chrien, N.C,L., CJ. Bruegge, and B.R. Barkstrom *(1993).* Estimation of calibration uncertainties for the Multi-angle Imaging SpectroRadiometer (MISR) via fidelity intervals. In *Sensor Systems for the Early Earth Observing System Platforms*, Proc. SPIE 1939, April, 114-125.

5. Jorquera, C.R., V.G. Ford, V.G. Duval, and CJ. Bruegge (1995). State of the art radiometer standards for NASA's Earth Observing System. Aerospace Applications Conference, 5- 10Feb, Snowmass, CO.

6. Biggar, S.F. and P.N. Slater (1993). Preflight cross-calibration radiometer for EOS AM-1 platform visible and near-IR sources. SPIE proc. 1939,243-249.

7. Sakuma, F., M. Kobayasi, and A. One. Aster round-robin radiometers for the preflight cros.calibration of EOS AM-1 instruments. Publication journal unknown.

η = bulb electrical to optical conversion efficiency (empirically determined to be 0.74);
Φ_{bulb} = electrical wattage per bulb type= 200 W (30 W);
σT^4 = total optical output of the bulb, integrated over wavelength, T=3220 K (31 OOK);
p = sphere reflectance= 0,98 for Spectraflec (adjusted to 0,966 for MISR Band 4);
f = ratio of non-reflecting area of sphere to total sphere area= 0.05;
$L_{BB\lambda}$ = spectral radiance from the sphere, as given by Planck's equation; and
A_s = sphere area= $\pi(1.65\ m)^2$.

For the satellite sphere $\Phi_{sat} = \frac{\Phi_{bulb}\rho f_{exit} V}{1-\rho(1-f_{sat})}$, where

F_{exit} = area of the exit port to surface area of sphere = 0.028; and
V= view factor= 0.69.

By using this model, the total sphere output was determined by summing over the radiance per bulb type and number of bulbs on, as well as scaling by the satellite sphere aperture. The bulb efficiency was scaled to provide a best fit of the data across the wavelength observations, The agreements of the original observations to the fit 0.4, -1.8, 0.8, and 1.3%. Next, the visitor radiance observations were compared to this model. A summary of the detector intercomparison observations is given in Table 4. The number of wavelength intercomparisons was limited because only the Band 2 MISR detector standard was available at this date, and the NRLM radiometer is a single channel. The particular level studied had all lamps on, and the satellite sphere aperture fully open. With agreements being better than 1%, we have gained confidence in our fundamental approach.

Table 4. Radiances [W $m^{-2}sr^{-1}\mu m^{-1}$] as compared to the sphere model, and percentage deviation.

	Wavelength (nm)		
Radiometer	550	650	666
MISR	612. (0.4%)		
UofA	584. (1.%)		934 (-0.8%).
NRLM		(909) 0.9%	

4. Acknowledgments

The design, fabrication, and characterization of the MISR instrument is credited to a large number of individuals. The test and characterization plans described in this text have been developed with the assistance of S. Teré Smith (camera and system test engineer), Ghobi Saghri (spectral and radiometric testing), Carlos Jorquera (photodiode standard and flight diodes), Eric B. Hochberg (optical testing), Bidushi Bhattacharya (RCC data analysis and data custodian), Neil Pignatano (Ground Support Equipment), Mary White (tens fabrication and test), Enrique Villegas (CCD fabrication and test), Virginia Ford (camera and diode optomechanical design and fabrication), Jewel Beckert (Instrument managers), Don Rockey and Gary Francis (system engineers), Terrence H. Reilly (project manager), and David Diner (principal investigator). Stuart Biggar and Fumihiro Sakuma are thanked for supporting the round-robin intercomparison. The work described in this paper is being carried out by the Jet Propulsion Laboratory, California Institute of Technology, under contract with the National Aeronautics and Space Administration.

5. References

1. Korechoff, R.P., DJ. Diner, D. J. Preston, and C.J. Bruegge (1995). Spectroradiometer focal plane design considerations: lessons learned from MISR camera testing. In Sensors, Systems, and Next Generation Satellites, EurOpt, 25-29Sep, Pans, France (this issue).

2. Bruegge, C.J., DJ. Diner, and V.G. Duval (1995). The MISR calibration program. Accepted to J. of Atmos. and Oceanic' Tech., EOS special issue.